ACS central science

Research Article

http://pubs.acs.org/journal/acscii

Concerted One-Electron Two-Proton Transfer Processes in Models Inspired by the Tyr-His Couple of Photosystem II

Mioy T. Huynh,[†,‡] S. Jimena Mora,[‡,§] Matias Villalba,[§] Marely E. Tejeda-Ferrari,[§] Paul A. Liddell,[§] Brian R. Cherry,[§] Anne-Lucie Teillout,[∥] Charles W. Machan,[⊥] Clifford P. Kubiak,[#] Devens Gust,[§] Thomas A. Moore,[§] Sharon Hammes-Schiffer,[*,†] and Ana L. Moore[*,§]

[†]Department of Chemistry, University of Illinois at Urbana−Champaign, 600 South Mathews Avenue, Urbana, Illinois 61801, United States

[§]School of Molecular Sciences, Arizona State University, Tempe, Arizona 85287, United States

[∥]Laboratoire de Chimie Physique, Groupe d'Electrochimie et de Photoélectrochimie, UMR 8000 CNRS, Université Paris-Sud, Batiment 350, 91405 Orsay Cedex, France

[⊥]Department of Chemistry, University of Virginia, McCormick Road, PO 400319, Charlottesville, Virginia 22904, United States

[#]Department of Chemistry and Biochemistry, University of California, San Diego, 9500 Gilman Drive, MC 0358, La Jolla, California 92093, United States

Supporting Information

ABSTRACT: Nature employs a Tyr_Z-His pair as a redox relay that couples proton transfer to the redox process between P680 and the water oxidizing catalyst in photosystem II. Artificial redox relays composed of different benzimidazole−phenol dyads (benzimidazole models His and phenol models Tyr) with substituents designed to simulate the hydrogen bond network surrounding the Tyr_Z-His pair have been prepared. When the benzimidazole substituents are strong proton acceptors such as primary or tertiary amines, theory predicts that a concerted two proton transfer process associated with the electrochemical oxidation of the phenol will take place. Also, theory predicts a decrease in the redox potential of the phenol by ∼300 mV and a small kinetic isotope effect (KIE). Indeed, electrochemical, spectroelectrochemical, and KIE experimental data are consistent with these predictions. Notably, these results were obtained by using theory to guide the rational design of artificial systems and have implications for managing proton activity to optimize efficiency at energy conversion sites involving water oxidation and reduction.

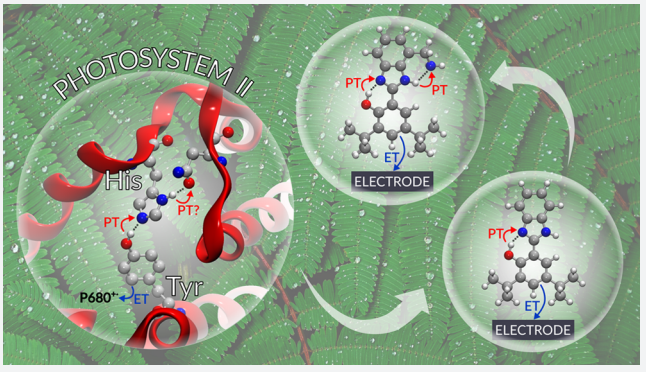

1. INTRODUCTION

In photosystem II (PSII) Tyr_Z (Y_Z) acts as a redox mediator between the oxidized primary electron donor, $P680^{\bullet+}$, and the oxygen evolving complex (OEC), a Mn_4CaO_5 cluster where water oxidation takes place. By providing an interface between the fast photoinitiated steps of photosynthesis and the slow catalytic process of water oxidation, Y_Z is thought to be an important factor contributing to the high photochemical quantum efficiency of PSII.[1,2] It is known that upon oxidation Y_Z donates a proton to its hydrogen-bonded partner, His-190, and that the thermodynamic activity of this proton is crucial for preserving the high redox potential necessary for water oxidation. This is one of the most widely cited proton-coupled electron transfer (PCET) processes in natural systems.[3−9]

This reaction has also been proposed to play an essential thermodynamic role in the generation of proton motive force (PMF). In 2000, Tommos and Babcock wrote, "it is at the level of Y_Z that proton currents are switched on", and hypothesized that, instead of a single proton transfer upon oxidation of Y_Z, a series of proton transfers can be associated with the oxidation of the phenol, culminating with proton release into the lumen contributing to the PMF.[1] In agreement with this hypothesis, a possible proton channel from the OEC through Y_Z and extending to the thylakoid lumen was identified in the 1.9 Å resolution crystal structure of PSII obtained by Umena et al.[10] However, the issue of proton channels within PSII remains controversial, and the identification of functional proton pathways in the water oxidation cycle is an active area of theoretical and experimental research. Several proton pathways have been proposed, consisting of networks of hydrogen-bonded polar residues and water molecules, where protons can diffuse by a Grotthuss-type mechanism spanning the ∼20 Å distance between the OEC and the lumen.[11−14] It is

Received: March 21, 2017
Published: May 9, 2017

DOI: 10.1021/acscentsci.7b00125
ACS Cent. Sci. 2017, 3, 372−380

unambiguous, however, that the protons liberated upon water oxidation find their way to the lumen, where they contribute to the PMF across the thylakoid membrane.

The design, synthesis, and study of simple systems where multiple proton transfers can be associated with the oxidation of a phenol in a concerted mechanism is a challenging but worthwhile endeavor. In addition to providing a deeper understanding of natural systems such as PSII, these studies help to establish design principles for controlling proton activity at catalytic water oxidation sites in artificial photosynthesis, where managing proton activity is thought to be key to efficient catalysis.[15−17] Costentin et al. demonstrated two protons transferring concertedly with one electron transfer using an intramolecular contiguous alcohol proton relay induced by oxidation.[18−21] Herein, we provide theoretical and experimental evidence in biomimetic constructs consisting of benzimidazole phenols (BIPs) substituted with amino groups (see Figure 1 for the example of BIP-CH_2NEt_2) for a concerted

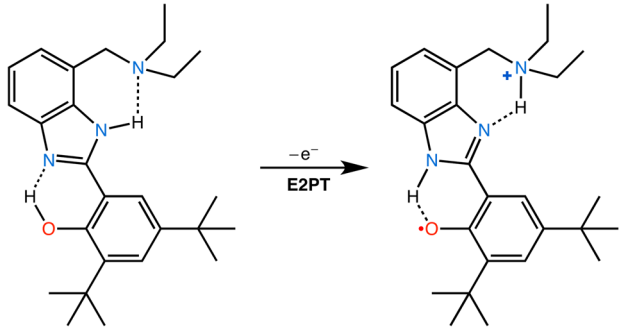

Figure 1. A bioinspired system: substituted benzimidazole phenol (BIP-CH_2NEt_2), consisting of a phenol internally hydrogen bonded to a benzimidazole proximal nitrogen and a secondary proton acceptor, a tertiary amine, that is hydrogen bonded to the distal NH of the benzimidazole. Upon electrochemical oxidation of the phenol, the system undergoes two concerted proton transfer reactions, resulting in a phenoxyl radical and an ammonium ion.

one-electron two-proton transfer (E2PT) process that takes place when the phenol is oxidized electrochemically. We call this process E2PT to differentiate it from the EPT process that describes a concerted one-electron one-proton transfer process. The E2PT process shown in Figure 1 results in the translocation of protons over a distance of ca. 7 Å and is a starting point for the design of bioinspired proton wires. Although oxidation of the phenol in the amino-BIPs reported here was electrochemically driven, the E2PT process could be light-driven by substituting the BIP of photochemically activated triad systems previously reported by amino-BIPs.[2,22−24]

2. RESULTS AND DISCUSSION

2.1. Synthesis and Characterization. Benzimidazole phenol derivatives (BIPs, Figure 2) have been chosen to examine the mechanism of proton transfer that accompanies the oxidation of the phenol moiety, and to validate the theoretical prediction of a lowered redox potential for a concerted one-electron two-proton reaction (*vide infra*). Different substitutions on the BIP allow for the interrogation of both one- and two-proton transfer reactions paired with a redox event on a single molecular platform. Substituted BIPs (Figure 2) were synthesized by a modification of the standard

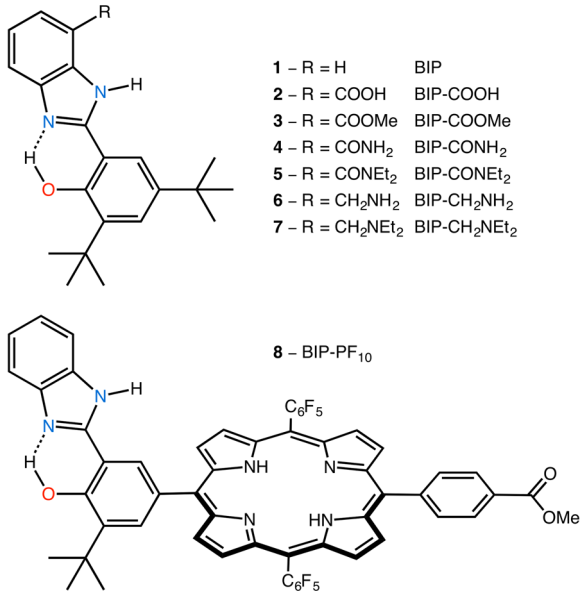

Figure 2. Benzimidazole phenol derivatives (BIPs) of the present study.

procedure (Supporting Information, synthesis) with *o*-phenylenediamine or its carbomethoxy derivative and the complementary *o*-hydroxybenzaldehyde derivative as starting substrates for the Philipps−Ladenburg reaction.[22,25,26] Amide **4** was prepared by aminolysis of **3**, and amide **5** was prepared by a coupling reaction starting with **2** and diethylamine with 1-ethyl-3-(3-(dimethylamino)propyl)carbodiimide (EDCI) as a coupling reagent. The reduction of **4** and **5** with $LiAlH_4$ generated the corresponding amines, **6** and **7**.

The presence of a strong intramolecular hydrogen bond involving the phenol and the nitrogen lone pair of benzimidazole (~2.5 Å O−N distance) is well established,[2,27] and NMR data for **1**−**7** support such a bond in these cases. Evidence for the formation of a hydrogen bond between the distal NH of benzimidazole and the benzylamine nitrogen (Figure 1) comes from the NMR chemical shift of the distal NH group of benzimidazole. The chemical shift of benzimidazole NH varies considerably with solvent, shifting downfield by about 2.5 ppm from chloroform to acetone. This change is attributed to the formation of hydrogen bonds with the solvent in the case of acetone.[2] In **7** the ^{1}H resonance of the benzimidazole NH is found at 11.17 ppm in chloroform, considerably downfield compared to the equivalent NH in **1** (9.34 ppm),[22] and does not shift over 10-fold changes in concentration. Additional support for the formation of the hydrogen bond between the distal NH of benzimidazole and the exocyclic amine nitrogen comes from IR data, where a shift to lower frequencies is observed for the stretching and bending vibrations involving the NH compared with **1** (Figure 5B and Figures S28 and S31).

Because of the unsymmetrical benzimidazole group, any BIP substituted at the 4 position (i.e., compounds **2**−**7** in Figure 2) consists of a mixture of two isomers due to tautomerization of the imidazole and rotation around the bond between the benzimidazole and the phenol moieties. Because their interconversion is slow on the NMR time scale (lifetime of the isomers is >200 ms as measured for BIP-5-CH_3), their presence and ratio can be clearly detected by ^{1}H NMR. Only one of the isomers has the two internal hydrogen bonds

DOI: 10.1021/acscentsci.7b00125
ACS Cent. Sci. 2017, 3, 372−380

necessary for E2PT; it is shown above for **7** (Figure 1) where the OH is hydrogen bonded to the lone pair of the benzimidazole nitrogen and a second internal hydrogen bond exists between the lone pair of the exocyclic NEt_2 group and the distal NH of the benzimidazole. The other isomer (not shown) lacks the hydrogen bond between the distal NH of the benzimidazole and the NEt_2. The ratio of isomers is approximately 1:1.5 in the case of **7** in acetonitrile as determined by ^{1}H NMR (Figure S22).

2.2. Electrochemical Evidence for a Concerted E2PT Process in BIP-CH_2NH_2 (6) and BIP-CH_2NEt_2 (7). The redox potentials for compounds **1**−**8** were calculated with DFT using previously benchmarked methods described elsewhere,[28] and the predicted values were subsequently found to be consistent with the experimental measurements (Table 1). For most of the BIP compounds (**1**−**5** and **8**), the predicted and experimental redox potentials are ∼0.9−1.0 V vs SCE in acetonitrile and correspond to the concerted oxidation of the phenol and transfer of the phenolic proton to the benzimidazole (an EPT process). For **6** and **7**, the oxidation of the phenol was predicted by DFT to occur concertedly with the transfer of *both* the phenolic and distal benzimidazole protons (an E2PT process) on the basis of a thermodynamic analysis, as discussed below. Moreover, prior to experimental measurements, the DFT calculations predicted that this concerted two-proton transfer would shift the potentials by approximately 300 mV to less positive values (∼0.6 V vs SCE) in **6** and **7**.

Table 1. Calculated and Experimental First Redox Potentials for the Phenol of BIPs

	$E_{1/2}$ (V vs SCE)	
compound	calculated	experimental
1: BIP	1.04[a]	1.04[b]
2: BIP-COOH	0.98	0.90
3: BIP-COOMe	0.96	0.93
4: BIP-$CONH_2$	0.94	0.92
5: BIP-$CONEt_2$	0.95	0.92
6: BIP-CH_2NH_2	0.66	0.56
7: BIP-CH_2NEt_2	0.57	0.54
8: BIP-PF_{10}	0.94	1.00[b]
9: BIP-Ph^{H}imine[c]	0.84	n/a
10: BIP-Ph^{Me}imine[c]	0.82	n/a
11: BIP-Ph^{Cl}imine[c]	0.88	n/a

[a]This couple was used as the reference for all other calculated potentials, so it agrees with the experimental value by construction. In this procedure, the redox potentials for **2**−**11** were calculated relative to the redox potential of **1**, which was shifted to agree with the experimental value (i.e., the difference between the experimental and calculated values for **1** was added to all calculated potentials). [b]Experimental data from ref 2. [c]For the structures of **9**−**11** see Figure S1.

This theoretical prediction is corroborated experimentally (see Table 1 and Figure 3A). The cyclic voltammograms (CVs) of the amino substituted BIPs exhibit a midpoint potential approximately 300 mV less positive than that of the other BIPs. The waves are quasi-reversible in acetonitrile solution with a peak-to-peak separation of ∼100 mV. Good evidence that the observed redox waves at 0.56 and 0.54 V vs SCE for **6** and **7**, respectively, correspond to the oxidation of the phenol comes from the comparison with the redox characteristics of the reference compounds lacking the phenol group, benzylamine and diethylbenzylamine, which exhibit irreversible oxidation waves at 1.45 and 0.85 V vs SCE, respectively, and thus are substantially different from **6** and **7** (Figure S23A,B). Furthermore, titration with trifluoracetic acid (TFA) of a solution of **7** in dichloromethane (Figure 3B and Figure S25B) clearly shows the disappearance of the wave at ∼0.6 V vs SCE associated with the E2PT process, and at 2 mM TFA the appearance of the wave typical of the EPT process observed for BIPs **1**−**5** listed in Table 1. These results are explained by protonation of the exocyclic amino group by TFA (pK_a ∼ 13 in acetonitrile) in either **6** (primary amino group pK_a ∼ 17 in acetonitrile) or **7** (tertiary amino group pK_a ∼ 19 in acetonitrile), which eliminates the exocyclic amino group as a thermodynamically competent secondary proton acceptor.[29−31] At even higher concentrations of TFA, the electrochemical oxidation of the protonated benzimidazole group can be detected at ∼1.4 and 1.5 V vs SCE for **6** and **7**, respectively (Figure S25A,B).[32]

The absence of two proton transfers associated with the single electron oxidation of the phenol for **2**−**5** can be explained on thermodynamic grounds. The pK_as in acetonitrile

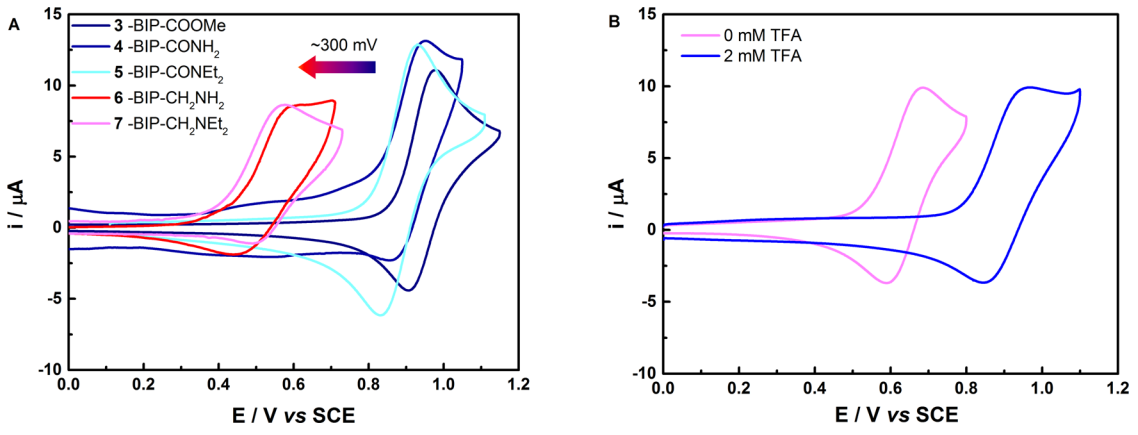

Figure 3. (A) CVs of BIPs. Concentration: 1 mM of the indicated BIPs, 0.5 M $TBAPF_6$ in dry acetonitrile. WE: glassy carbon. RE: Ag/AgCl (Fc as internal reference). CE: Pt. Note that **3**, **4**, and **5** do not oxidize at 0.7 V vs SCE. (B) CVs of **7** before and after the addition of 2 equiv of TFA in dry dichloromethane. Concentration of **7**, 1 mM, 0.5 M $TBAPF_6$ supporting electrolyte. WE: glassy carbon. RE: Ag/AgCl (Fc as internal reference). CE: Pt. Sweep rate, 100 mV s^{-1}.

DOI: 10.1021/acscentsci.7b00125
ACS Cent. Sci. 2017, 3, 372−380

of the protonated carbonyl groups of **2** and **3** are ≤0, and those of **4** and **5** are ∼4,[33] which is much lower than the pK_a of the benzimidazolium ion in acetonitrile (∼14).[30] Therefore, a second proton transfer is thermodynamically unfavorable. The calculated free energy differences[28] between the oxidized product after double proton transfer and the oxidized product after single proton transfer are given in Table 2. These values indicate that when the BIPs are substituted with better proton acceptors such as primary or tertiary amines, the second proton transfer becomes thermodynamically favorable, and an E2PT process could occur.

Table 2. Calculated ΔG° between Double and Single PT Oxidized States[a]

oxidized species	ΔG° (kcal/mol)
2: BIP-COOH$^{\bullet+}$	15.2
3: BIP-COOMe$^{\bullet+}$	14.9
4: BIP-CONH$_2^{\bullet+}$	7.1
5: BIP-CONEt$_2^{\bullet+}$	5.6
6: BIP-CH$_2$NH$_2^{\bullet+}$	−4.2
7: BIP-CH$_2$NEt$_2^{\bullet+}$	−6.5
9: BIP-Ph^{H}imine$^{\bullet+}$	−2.9
10: BIP-Ph^{Me}imine$^{\bullet+}$	−3.1
11: BIP-Ph^{Cl}imine$^{\bullet+}$	−2.1

[a]The reported values are the free energy differences between the oxidized state with and without the second proton transfer. The double proton transfer corresponds to proton transfer from the phenol to the proximal imidazole N and proton transfer from the distal imidazole NH to the R group, while the single proton transfer corresponds to only the first proton transfer. Negative values for ΔG° indicate that the double proton transfer is more thermodynamically favorable than the single proton transfer. No values are reported for **1** and **8** because only a single proton transfer is possible. Using the experimental pK_as (*vide supra*)[29−31] for the benzimidazole and exocyclic amines in acetonitrile we estimated ΔG° = −3.9 kcal/mol for **6** and −6.5 kcal/mol for **7**, in good agreement with the calculated values.

The thermodynamic price paid for the E2PT process in **6** and **7** is the loss of ∼300 mV in the redox potential of the phenol, indicating that neither could be used to oxidize a catalyst for water oxidation at near-neutral to acidic pH. This price must be a function of the ΔpK_a between the proton acceptor and donor for the second proton transfer (i.e., the pK_a difference between the protonated exocyclic amine and the distal NH of the benzimidazolium ion). Encouragingly, however, theoretical calculations predict that substituents with reduced pK_as, such as substituted imines attached to BIP (see **9**−**11** in Tables 1 and 2 and Figure S1), would still undergo concerted E2PT but maintain a considerably higher potential for the phenol oxidation.

It is interesting to consider the implications of these findings for the phenolic proton of the Tyr$_Z$-His pair in photosynthesis. If the phenolic proton is pumped into the lumen and the phenol is "reloaded" with a proton from ongoing water oxidation, the ΔpK_a between the His and lumen must be less than that of **6** and **7** in order for the redox relay to be able to oxidize the OEC. This ΔpK_a is a function of the proton electrochemical potential (in the Michelian sense) inside the lumen, and could maintain the redox poise sufficient to oxidize the OEC.[34] Alternatively, if the phenolic proton is not pumped into the lumen, but remains shared between the phenoxyl radical and its His hydrogen-bonded partner, the surroundings could modulate the ΔpK_a to maintain the necessary redox potential. This mechanism has been proposed and is known as proton rocking.[35,36] As alluded to in the Introduction, regardless of mechanistic details, this proton is a key player in water oxidation and the concomitant generation of the PMF in photosynthetic membranes.

2.3. Infrared Spectroelectrochemistry. Infrared spectroelectrochemistry (IRSEC) allows for the identification of bonding changes due to redox-linked protonation/deprotonation of specific sites in the molecules during the PCET process. For example, in the IRSEC spectra obtained for **1** at a potential of 1.0 V vs SCE, protonation of the benzimidazole moiety upon oxidation of the phenol can be easily detected by the decrease in the intensity of the bands at 3453 and 3415 cm^{-1}, which correspond to the NH stretching of the benzimidazole moiety, and the concomitant appearance of the band at 3323 cm^{-1}, which corresponds to the NH stretching of the benzimidazolium ion (Figure S26A).[27,37] In agreement with this observation, similar changes were detected in this region of the IR spectrum when a solution of **1** was treated with gaseous HCl (Figure S26B).

Figure 4A shows the IRSEC spectra of **1** at lower frequencies (1700−1300 cm^{-1}), where large changes in absorbance are

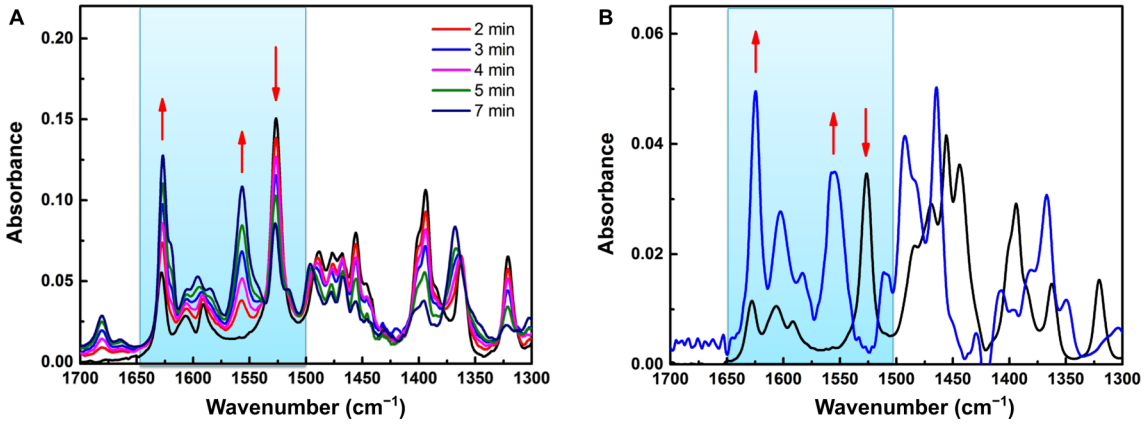

Figure 4. (A) Time course of the IRSEC spectra of **1** (19 mM) obtained at a potential of 1.0 V vs SCE. The spectrum of **1** obtained at resting potential is shown in black. Solvent dichloromethane, 0.1 M TBAPF$_6$. (B) IR spectra of **1**, neutral (black) and protonated with gaseous HCl (blue). Solvent dichloromethane.

DOI: 10.1021/acscentsci.7b00125
ACS Cent. Sci. 2017, 3, 372−380

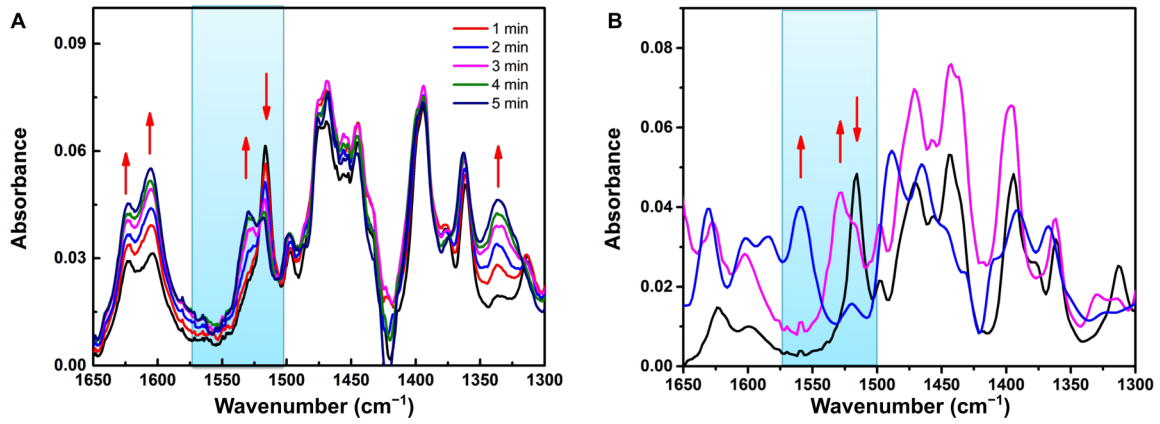

Figure 5. (A) Time course of the IRSEC spectra of **7** (17 mM) obtained at a potential of 0.7 V vs SCE. The spectrum of **7** obtained at resting potential is shown in black. Solvent dichloromethane, 0.1 M $TBAPF_6$. (B) Spectra of **7** neutral (black), tertiary exocyclic amine protonated with 2 equiv of TFA (pink), and protonated with excess gaseous HCl (blue). Solvent dichloromethane.

indicated with upward (increasing intensity) and downward (decreasing intensity) arrows when a potential of 1.0 V vs SCE was applied. Many of the changes observed are similar to those observed in the IR spectrum of **1** when it is treated with gaseous HCl (see the bands at 1626, 1556, and 1526 cm^{-1}, red arrows in Figure 4B). For example, the band at 1626 cm^{-1} increases considerably both under the applied potential and following protonation by treatment of **1** with HCl. This band has a large component of the C═N stretching vibration of the benzimidazole, for which the dipole moment increases upon protonation.[37] However, some mismatches are expected between the IR and the IRSEC spectra because the IRSEC detects the bonding changes associated with the formation of the phenoxyl radical and the associated proton transfer (the EPT process), whereas the treatment with HCl only affords a protonation state mimicking the product of the EPT process without the ET. For example, a new band at 1556 cm^{-1} grows in both spectra when a potential of 1.0 V vs SCE is applied (Figure 4A) and when **1** is protonated by treatment with gaseous HCl (Figure 4B); however, the band at ∼1526 cm^{-1} decreases in intensity under the applied potential (Figure 4A) but disappears upon protonation (Figure 4B). The band at 1556 cm^{-1} includes an NH in-plane bending vibration in the benzimidazolium ion, while the band at 1526 cm^{-1} includes an NH in-plane bending mode of the benzimidazole that includes a considerable contribution from the phenoxyl radical, as supported by DFT normal-mode analysis (Figures S35 and S36).[37−39] Both of these bands exhibit clear shifts to lower wavenumbers upon deuteration (Figures S32A,B). In summary, considering the close correlation between the IRSEC and the IR data, it can be concluded that protonation of BIP by HCl acid and by the EPT process produces similar changes in the bonding around the benzimidazole moiety, namely, the formation of the benzimidazolium ion.

Because the redox potentials of **6** and **7** are ∼300 mV lower than those of BIPs **1**−**5**, the changes in the IRSEC spectra of **6** and **7** are expected to occur at significantly lower potentials than those of the other BIPs. As predicted, the IRSEC spectrum of **1** does not show any changes when a potential of 0.7 V vs SCE was applied (Figure S29A,B), while the IRSEC spectrum of **7** shows significant changes over several minutes at this potential, the results of which are described below.

In the IRSEC spectrum of **7** obtained at zero applied potential, a band is observed at 3375 cm^{-1}, which corresponds to the stretching mode of the benzimidazole NH (Figure S28A). The shift of the NH stretching mode from ∼3430 cm^{-1} in **1** to 3375 cm^{-1} in **7** can be interpreted as a weakening of the benzimidazole NH bond due to the formation of the internal hydrogen bond with the exocyclic tertiary amine. When a potential of 0.7 V vs SCE is applied in the case of **7**, two new bands grow in at ∼3460 and 3190 cm^{-1}, which are assigned to the stretching modes of the proximal benzimidazole NH and the NH of the exocyclic ammonium ion, respectively. These assignments are supported by the calculated normal modes for **7** (Figures S35 and S36). It is important to note that no indication of a benzimidazolium NH stretching band, observed at 3323 cm^{-1} for **1** after EPT, can be detected in the case of **7**.

In the region between 1700 and 1300 cm^{-1} no difference can be detected in the spectra of **1** taken at 0 and 0.7 V vs SCE (Figure S29B), as the EPT process is expected to occur at ∼1.0 vs SCE. Under comparable conditions for **7**, four distinct bands at 1622, 1604, 1529, and 1340 cm^{-1} increase in intensity, while the band at 1515 cm^{-1} decreases in intensity (Figure 5A). The band at 1515 cm^{-1} has a large component of the NH in-plane bending, comparable to the band at 1526 cm^{-1} of **1** but at lower frequency, in agreement with the presence of an internal hydrogen bond with the exocyclic amine. Importantly, there is no band growing in at 1556 cm^{-1} for **7**, which was clearly observed for **1** after EPT. This band corresponds to the formation of the benzimidazolium ion and can be observed in the IR spectrum of **7** only after treatment with excess gaseous HCl, where both the exocyclic amino group and the benzimidazole moiety are expected to be protonated (Figure 5B and Figure S31C).

The data in Figure 3B indicate that adding 2 equiv of TFA to a solution of **7** protonates the exocyclic amine, which disrupts the hydrogen bond with the distal NH of the benzimidazole and prevents this second proton transfer (Figure S31B). This process was monitored by the disappearance of the band at 1515 cm^{-1} and the concomitant appearance of the band at 1529 cm^{-1} (Figure 5B and Figure S33A). The band at 1529 cm^{-1} is characteristic of the benzimidazole NH bending vibration and upon deuteration shifts to 1506 cm^{-1} (Figure S33B). The IRSEC experiments (Figure 5A) show that the bands at 1515 and 1529 cm^{-1} change in the same manner upon oxidation of the phenol as they did in the TFA titration above. This behavior is consistent with protonation of both the exocyclic amine and the proximal N of the benzimidazole

DOI: 10.1021/acscentsci.7b00125
ACS Cent. Sci. 2017, 3, 372−380

(Figure S31D). These observations provide further evidence for the proposed E2PT process (Figure 1) in which the exocyclic amine and the proximal N of the benzimidazole are protonated but the distal N of the benzimidazole is not protonated after oxidation of the phenol in **7**.

2.4. KIE Calculations and Experimental Results. A kinetic isotope effect (KIE) is often regarded as the hallmark of reactions involving concerted PCET processes, although exceptions are possible.[40,41] Experimental KIE values were determined electrochemically and are reported in Table 3 along with theoretical values (*vide infra*). For the BIP derivatives **1**−**5** reported in this work, a KIE of ∼2 is expected if the PCET takes place by a concerted mechanism, according to studies of related systems.[27,42,43] In Table 3, the theoretical KIE values for compounds **1**−**5** correspond to a single proton transferred concertedly upon oxidation of the phenol (EPT). In the case of **6** and **7**, the calculated KIE values correspond to two protons transferred concertedly upon oxidation of the phenol (E2PT).

Table 3. Calculated and Experimental Kinetic Isotope Effects

	KIE	
compound	calculated[a]	experimental
1: BIP	1.9	n/a (1.4[b])
2: BIP-COOH	2.0	1.5 ± 0.3
3: BIP-COOMe	2.1	1.8 ± 0.3
4: BIP-$CONH_2$	1.8	1.7 ± 0.5
5: BIP-$CONEt_2$	2.0	n/a
6: BIP-CH_2NH_2	1.6	n/a
7: BIP-CH_2NEt_2	1.3	0.9 ± 0.5
8: BIP-PF_{10}[c]	1.0	1.0 ± 0.3

[a]The uncertainties of the calculated KIEs are approximately ±0.5 within this theoretical framework (Supporting Information, KIE). [b]Data for related compound from ref 43. [c]Supporting Information, BIP-PF_{10}.

We calculated the electrochemical rate constant using a general PCET theory.[44] In this treatment, the anodic nonadiabatic EPT rate constant for fixed proton donor−acceptor distance (R) is given by[45−47]

$$k^{\mathrm{EPT}}(\eta; R) = \sum_{\mu,\nu} P_\mu \frac{(V^{\mathrm{el}} S_{\mu\nu})^2}{\beta' \hbar} \sqrt{\frac{\pi}{\lambda k_{\mathrm{B}} T}} \rho_{\mathrm{M}} \int \mathrm{d}\varepsilon [1 - f(\varepsilon)] \exp\left[\frac{-\Delta G^{\ddagger}_{\mu\nu}}{k_{\mathrm{B}} T}\right] \quad (1)$$

where the double summation is over all pairs of reactant/product electron−proton vibronic states, P_μ is the Boltzmann probability for vibronic state μ, $f(\varepsilon)$ is the Fermi distribution function for the electronic states with energy ε in the electrode, ρ_{M} is the density of states at the Fermi level, V^{el} is the electronic coupling, β' is a parameter of magnitude ∼1 $Å^{-1}$ representing the exponential decay of V^{el} with distance, λ is the reorganization energy, $S_{\mu\nu}$ is the overlap integral between the proton vibrational wave functions μ and ν, and $\Delta G^{\ddagger}_{\mu\nu}$ is the free energy barrier associated with states μ and ν, which depends on the overpotential η. In eq 1, P_μ, $S_{\mu\nu}$, and $\Delta G^{\ddagger}_{\mu\nu}$ depend on the proton donor−acceptor distance R. A detailed explanation of how the parameters in eq 1 are defined and calculated is given in the Supporting Information (pages S39−S53).

To account for the proton donor−acceptor motion, the rate constant is thermally averaged over the proton donor−acceptor distance R:[40,48−50]

$$k^{\mathrm{EPT}}(\eta) = \int P(R) k^{\mathrm{EPT}}(\eta; R)\, \mathrm{d}R \quad (2)$$

Thus, the overall EPT rate constant is determined by calculating the rate constant at a series of R values and numerically integrating over R, weighting the rate constant by the probability $P(R)$ of sampling each R value. For a given pair of reactant/product (μ/ν) vibronic states, the rate constant is proportional to the square of the proton vibrational wave function overlap ($S_{\mu\nu}$), and the KIE is proportional to the square of the ratio of the overlaps for hydrogen and deuterium.[40,51] Typically, the KIE increases as the overlap decreases. However, the combined summation over all pairs of reactant/product vibronic states and the integration over R leads to more complex behavior that requires the complete calculation of the rate constant for each molecular system. This theoretical treatment has been extended to the case of concerted electron transfer with two proton transfers (E2PT), resulting in similar physical principles but additional complexity.[49]

KIEs were experimentally measured in the electrochemical oxidation of several of the phenols shown in Figure 2 (see Table 3 and Figure S34B). Overall, the calculated and experimentally measured KIE values are in good agreement, with both sets of KIE values showing similar trends across the BIP compounds studied. The KIE values obtained for BIPs **1**−**4** are relatively small but are in line with previously reported values for related systems.[27,43,52,53] A more detailed analysis of the KIEs is provided in the Supporting Information (pages S54−S61). The theoretical calculations lead to a KIE of unity for **8** because of dominant contributions from excited vibronic states with vibrational wave function overlaps that are nearly unity, mainly arising from the delocalization of the unpaired electron onto the porphyrin ring in the oxidized state. In contrast, the calculated KIEs of ∼2 for BIPs **1**−**5** arise because of dominant contributions from excited vibronic states with smaller vibrational wave function overlaps (∼0.5). In the case of **6** and **7**, where two proton transfers are associated with the oxidation of the phenol, the calculated KIE values, as well as the experimentally measured KIE for **7**, are slightly smaller than those of BIPs **1**−**5**.

In principle, the shift in the redox potentials for compounds **6** and **7** could arise from a stepwise mechanism, in which an EPT step is followed by very fast, thermodynamically favorable transfer of the second proton, leading to the E2PT product. Because the CVs cannot clearly distinguish between this stepwise mechanism and the concerted E2PT mechanism, we are unable to rule out this possibility definitively. However, the DFT calculations indicate that the concerted mechanism is thermodynamically favored over the stepwise mechanism by 4−7 kcal/mol for compounds **6** and **7** (Table 2). Moreover, for compound **7**, the calculated KIE assuming the concerted E2PT mechanism is in agreement with the experimental KIE, which is slightly lower than the KIEs for the BIP compounds undergoing an EPT process (**1**−**5**, Table 3), also supporting an E2PT mechanism for **7**. However, due to the error bars in both the experimental and calculated KIEs, this agreement does not provide conclusive evidence of a specific mechanism. All of these data point to either a concerted E2PT mechanism or a stepwise mechanism with an extremely short-lived intermediate, which could be viewed as virtually concerted on relevant time scales. Regardless of the detailed mechanism, the net process is

DOI: 10.1021/acscentsci.7b00125
ACS Cent. Sci. 2017, 3, 372−380

the transfer of two protons upon oxidation of the BIP, producing the E2PT product, for compounds **6** and **7**.

3. CONCLUSION

In this work, we explored fundamental principles involved in coupling a redox process to proton transfer(s) in a redox relay inspired by photosynthesis. Theory predicted that a concerted two-proton transfer process associated with the oxidation of a phenol that is hydrogen bonded to a benzimidazole−amine construct would reduce the redox potential of the phenol by ∼300 mV and have a low KIE. Electrochemical, spectroelectrochemical, and KIE experimental data provide strong evidence that this E2PT process has indeed been observed. This is a powerful example of the predictive potential of theory, which clearly can be used to guide the rational design of artificial systems for energy conversion.

Protons are important in myriad ways for solar fuel production, beginning with their role in the catalysis of water oxidation to yield oxygen, protons, and reducing equivalents and ending with their role in the production of reduced carbon or hydrogen as fuels.[15,36] Managing proton activity is key to achieving low overpotentials for proton-linked redox reactions and to providing the "redox leveling" necessary for carrying out redox reactions involving multiple electrons coupled to a fixed redox source.[54] This study also helps address the thermodynamic consequences associated with the loss of the proton on Y_Z of PSII to the lumen in natural photosynthesis, as well as the thermodynamic cost in redox energy of moving protons in PCET processes via proton diffusion through a hydrogen-bonded network.

4. METHODS

4.1. Theoretical. The geometry optimizations and proton potentials were calculated with density functional theory (DFT) using the B3LYP functional and a 6-31G** basis set. Solvent effects were included using a conductor-like polarizable continuum model. All calculations were performed with *Gaussian 09*. Further computational details are provided in the Supporting Information.

4.2. Experimental Section. *4.2.1. Cyclic Voltammetry.* Cyclic voltammetry was performed with a CHI 650C potentiostat (CH Instrument) with scan rate of 0.1 V s^{-1}. A custom glass cell with Teflon top accommodating a three-electrode setup and 4 mL of solution was used. The working electrode was glassy carbon (3 mm diameter) polished with alumina (1 μm), thoroughly rinsed with ethanol and dried. The counter electrode was a platinum grid, and Ag/AgCl was used as a pseudoreference electrode, which was placed as close as possible to the working electrode in order to minimize the ohmic drop. All the potentials were corrected using the ferrocenium−ferrocene redox couple as an internal standard (with E_m taken as 0.31 V vs SCE in acetonitrile and 0.45 V vs SCE in dichloromethane). The compound of interest was dissolved at a concentration of 1 mM in acetonitrile or dichloromethane previously distilled and kept over molecular sieves and K_2CO_3. Tetrabutylammonium hexafluorophosphate ($TBAPF_6$) was kept in an oven overnight and then used as a supporting electrolyte for all experiments at a concentration of 0.5 M. The solution was purged with argon for 2 min prior to any experiment, and measurements were then taken under an argon atmosphere.

4.2.2. Infrared Spectroelectrochemistry (IRSEC) and FTIR. The experimental setup and design of the IRSEC cell has been published by the Kubiak Lab.[55,56] A Pine Instrument Company model AFCBP1 potentiostat was employed. As the potential was scanned, thin layer bulk electrolysis was monitored by Fourier-transform reflectance IR off the working electrode's surface. All experiments were conducted in 0.1 M $TBAPF_6$/dichloromethane solutions with analyte concentrations of ∼3 mM (unless otherwise noted) prepared under a nitrogen atmosphere. The IRSEC cells used (working electrode/reference electrode/counter electrode) were glassy carbon/Ag/Pt, meaning that all potentials were in reference to a pseudoreference electrode, bare metal Ag/Ag^+ (∼+200 mV from the Fc/Fc^+ couple).[55−57]

FTIR spectra were obtained in a Bruker Vertex 70 using a CaF_2 liquid transmission cell. The solvent (dichloromethane) was distilled over CaH_2 and kept over molecular sieves and K_2CO_3. The compounds were dried under high vacuum overnight.

4.2.3. KIE Determination. Variable scan rate cyclic voltammetry of the compounds at scan rates varying from 0.1 to 500 V s^{-1} in dry acetonitrile was used to determine the KIEs with a potentiostat/galvanostat model 273A (EG&G Princeton Applied Research) using a glassy carbon rod (Tokai 1 mm diameter) as a working electrode, a platinum grid as a counter electrode, and a Ag/AgCl pseudoreference electrode in a conventional three-electrode cell. To measure the apparent rate constant of the redox process, the electron transfer (ET) rate must be separated from the rates of diffusion processes. This is accomplished by increasing the scan rate until ET becomes rate determining. The peak potential separation is measured as a function of the scan rate. This peak separation is used to construct the "trumpet plot" from which the apparent standard rate constant was determined using the DigiSim software.

The apparent standard rate constants were determined for the compounds dissolved in acetonitrile containing 2% (v/v) of either CH_3OH or CH_3OD methanol. The experimental KIE is estimated by the ratio of these apparent rate constants (k_{appH}/k_{appD}).

■ ASSOCIATED CONTENT

Supporting Information

The Supporting Information is available free of charge on the ACS Publications website at DOI: 10.1021/acscentsci.7b00125.

Synthetic details; NMR, IR, IRSEC, electrochemical data; computational details; calculated redox potentials, IR spectra, free energies, and KIEs; analysis of rate constants; optimized Cartesian coordinates of all compounds studied (PDF)

■ AUTHOR INFORMATION

Corresponding Authors

*E-mail: shs3@illinois.edu.
*E-mail: amoore@asu.edu.

ORCID

Mioy T. Huynh: 0000-0002-0472-7624
Clifford P. Kubiak: 0000-0003-2186-488X
Sharon Hammes-Schiffer: 0000-0002-3782-6995

Author Contributions

‡M.T.H and S.J.M. contributed equally.

DOI: 10.1021/acscentsci.7b00125
ACS Cent. Sci. 2017, 3, 372−380

Notes

The authors declare no competing financial interest.

■ ACKNOWLEDGMENTS

This work was supported by the Office of Basic Energy Sciences, Division of Chemical Sciences, Geosciences, and Energy Biosciences, Department of Energy, under Contract DE-FG02-03ER15393. The computational portion of this work was supported as part of the Center for Molecular Electrocatalysis, an Energy Frontier Research Center funded by the U.S. Department of Energy, Office of Science, Office of Basic Energy Sciences (S.H.-S., M.T.H.), and a National Science Foundation Graduate Research Fellowship Grant (DGE-1144245, M.T.H.). C.W.M. and C.P.K. acknowledge support for this work from the AFOSR through a Basic Research Initiative (BRI) grant (FA9550-12-1-0414).

■ REFERENCES

(1) Tommos, C.; Babcock, G. T. Proton and hydrogen currents in photosynthetic water oxidation. *Biochim. Biophys. Acta, Bioenerg.* **2000**, *1458*, 199−219.
(2) Megiatto, J. D., Jr.; Méndez-Hernández, D. D.; Tejeda-Ferrari, M. E.; Teillout, A.-L.; Llansola Portoles, M. J.; Kodis, G.; Poluektov, O. G.; Rajh, T.; Mujica, V.; Groy, T. L.; Gust, D.; Moore, T. A.; Moore, A. L. A bioinspired redox relay that mimics radical interactions of the Tyr−His pairs of photosystem II. *Nat. Chem.* **2014**, *6*, 423−428.
(3) Keough, J. M.; Jenson, D. L.; Zuniga, A. N.; Barry, B. A. Proton coupled electron transfer and redox-active tyrosine Z in the photosynthetic oxygen-evolving complex. *J. Am. Chem. Soc.* **2011**, *133*, 11084−11087.
(4) Barry, B. A. Reaction dynamics and proton coupled electron transfer: Studies of tyrosine-based charge transfer in natural and biomimetic systems. *Biochim. Biophys. Acta, Bioenerg.* **2015**, *1847*, 46−54.
(5) Migliore, A.; Polizzi, N. F.; Therien, M. J.; Beratan, D. N. Biochemistry and theory of proton-coupled electron transfer. *Chem. Rev.* **2014**, *114*, 3381−3465.
(6) Sjödin, M.; Styring, S.; Åkermark, B.; Sun, L.; Hammarström, L. The mechanism for proton-coupled electron transfer from tyrosine in a model complex and comparisons with Y(Z) oxidation in photosystem II. *Philos. Trans. R. Soc., B* **2002**, *357*, 1471−1479.
(7) Faller, P.; Goussias, C.; Rutherford, A. W.; Un, S. Resolving intermediates in biological proton-coupled electron transfer: A tyrosyl radical prior to proton movement. *Proc. Natl. Acad. Sci. U. S. A.* **2003**, *100*, 8732−8735.
(8) Rappaport, F.; Boussac, A.; Force, D. A.; Peloquin, J.; Brynda, M.; Sugiura, M.; Un, S.; Britt, R. D.; Diner, B. A. Probing the coupling between proton and electron transfer in photosystem II core complexes containing a 3-fluorotyrosine. *J. Am. Chem. Soc.* **2009**, *131*, 4425−4433.
(9) Hammarström, L.; Styring, S. Proton-coupled electron transfer of tyrosines in Photosystem II and model systems for artificial photosynthesis: The role of a redox-active link between catalyst and photosensitizer. *Energy Environ. Sci.* **2011**, *4*, 2379−2388.
(10) Umena, Y.; Kawakami, K.; Shen, J.-R.; Kamiya, N. Crystal structure of oxygen-evolving photosystem II at a resolution of 1.9 Å. *Nature* **2011**, *473*, 55−60.
(11) Vogt, L.; Vinyard, D. J.; Khan, S.; Brudvig, G. W. Oxygen-evolving complex of photosystem II: An analysis of second-shell residues and hydrogen-bonding networks. *Curr. Opin. Chem. Biol.* **2015**, *25*, 152−158.
(12) Bondar, A.-N.; Dau, H. Extended protein/water H-bond networks in photosynthetic water oxidation. *Biochim. Biophys. Acta, Bioenerg.* **2012**, *1817*, 1177−1190.
(13) de Grotthuss, C. J. T. Mémoire sur la décomposition de l'eau et des corps qu'elle tient en dissolution à l'aide de l'électricité galvanique. *Ann. Chim. (Paris)* **1806**, *58*, 54−74.
(14) Agmon, N. The Grotthuss mechanism. *Chem. Phys. Lett.* **1995**, *244*, 456−462.
(15) Gagliardi, C. J.; Vannucci, A. K.; Concepcion, J. J.; Chen, Z.; Meyer, T. J. The role of proton coupled electron transfer in water oxidation. *Energy Environ. Sci.* **2012**, *5*, 7704−7717.
(16) Dogutan, D. K.; McGuire, R., Jr.; Nocera, D. G. Electocatalytic water oxidation by cobalt(III) hangman β-octafluoro corroles. *J. Am. Chem. Soc.* **2011**, *133*, 9178−9180.
(17) Matheu, R.; Ertem, M. Z.; Benet-Buchholz, J.; Coronado, E.; Batista, V. S.; Sala, X.; Llobet, A. Intramolecular proton transfer boosts water oxidation catalyzed by a Ru complex. *J. Am. Chem. Soc.* **2015**, *137*, 10786−10795.
(18) Costentin, C.; Robert, M.; Savéant, J.-M.; Tard, C. Inserting a hydrogen-bond relay between proton exchanging sites in proton-coupled electron transfers. *Angew. Chem., Int. Ed.* **2010**, *49*, 3803−3806.
(19) Costentin, C.; Robert, M.; Savéant, J.-M.; Tard, C. H-bond relays in proton-coupled electron transfers. Oxidation of a phenol concerted with proton transport to a distal base through an OH relay. *Phys. Chem. Chem. Phys.* **2011**, *13*, 5353−5358.
(20) Savéant, J.-M. Electrochemical approach to proton-coupled electron transfers: Recent advances. *Energy Environ. Sci.* **2012**, *5*, 7718−7731.
(21) Bonin, J.; Costentin, C.; Robert, M.; Savéant, J.-M.; Tard, C. Hydrogen-bond relays in concerted proton electron transfers. *Acc. Chem. Res.* **2012**, *45*, 372−381.
(22) Moore, G. F.; Hambourger, M.; Gervaldo, M.; Poluektov, O. G.; Rajh, T.; Gust, D.; Moore, T. A.; Moore, A. L. A bioinspired construct that mimics the proton coupled electron transfer between $P680^+$ and the Tyr_z-His190 pair of photosystem II. *J. Am. Chem. Soc.* **2008**, *130*, 10466−10467.
(23) Megiatto, J. D., Jr.; Antoniuk-Pablant, A.; Sherman, B. D.; Kodis, G.; Gervaldo, M.; Moore, T. A.; Moore, A. L.; Gust, D. Mimicking the electron transfer chain in photosystem II with a molecular triad thermodynamically capable of water oxidation. *Proc. Natl. Acad. Sci. U. S. A.* **2012**, *109* (39), 15578−15583.
(24) Zhao, Y.; Swierk, J. R.; Megiatto, J. D., Jr.; Sherman, B.; Youngblood, W. J.; Qin, D.; Lentz, D. M.; Moore, A. L.; Moore, T. A.; Gust, D.; Mallouk, T. E. Improving the efficiency of water splitting in dye-sensitized solar cells by using a biomimetic electron transfer mediator. *Proc. Natl. Acad. Sci. U. S. A.* **2012**, *109*, 15612−15616.
(25) Preston, P. N. Synthesis, reactions, and spectroscopic properties of benzimidazoles. *Chem. Rev.* **1974**, *74*, 279−314.
(26) Megiatto, J. D., Jr.; Patterson, D.; Sherman, B. D.; Moore, T. A.; Gust, D.; Moore, A. L. Intramolecular hydrogen bonding as a synthetic tool to induce chemical selectivity in acid catalyzed porphyrin synthesis. *Chem. Commun.* **2012**, *48*, 4558−4560.
(27) Markle, T. F.; Rhile, I. J.; DiPasquale, A. G.; Mayer, J. M. Probing concerted proton−electron transfer in phenol−imidazoles. *Proc. Natl. Acad. Sci. U. S. A.* **2008**, *105*, 8185−8190.
(28) Solis, B. H.; Hammes-Schiffer, S. Proton-coupled electron transfer in molecular electrocatalysis: Theoretical methods and design principles. *Inorg. Chem.* **2014**, *53*, 6427−6443.
(29) Kaljurand, I.; Kütt, A.; Sooväli, L.; Rodima, T.; Mäemets, V.; Leito, I.; Koppel, I. A. Extension of the self-consistent spectrophotometric basicity scale in acetonitrile to a full span of 28 pK_a units: Unification of different basicity scales. *J. Org. Chem.* **2005**, *70*, 1019−1028.
(30) Nurminen, E. J.; Mattinen, J. K.; Lönnberg, H. Nucleophilic and acid catalysis in phosphoramidite alcoholysis. *J. Chem. Soc., Perkin Trans. 2* **2001**, 2159−2165.
(31) Muckerman, J. T.; Skone, J. H.; Ning, M.; Wasada-Tsutsui, Y. Toward the accurate calculation of pK_a values in water and acetonitrile. *Biochim. Biophys. Acta, Bioenerg.* **2013**, *1827*, 882−891.
(32) Moore, G. F.; Hambourger, M.; Kodis, G.; Michl, W.; Gust, D.; Moore, T. A.; Moore, A. L. Effects of protonation state on a tyrosine-histidine bioinspired redox mediator. *J. Phys. Chem. B* **2010**, *114*, 14450−14457.

DOI: 10.1021/acscentsci.7b00125
ACS Cent. Sci. 2017, 3, 372−380

(33) Izutsu, K. *Acid-base dissociation contants in dipolar aprotic solvents*; Blackwell Scientific Publications: Oxford, 1990; Chemical Data Series No. 35.
(34) Blankenship, R. E. *Molecular mechanisms of photosynthesis*, 2nd ed.; Wiley-Blackwell: Oxford, U.K., 2014.
(35) Eckert, H.-J.; Renger, G. Temperature dependence of $P680^+$ reduction in O_2-evolving PS II membrane fragments at different redox states S_i of the water oxidizing system. *FEBS Lett.* **1988**, *236*, 425−431.
(36) Meyer, T. J.; Huynh, M. H.; Thorp, H. H. The possible role of proton-coupled electron transfer (PCET) in water oxidation by photosystem II. *Angew. Chem., Int. Ed.* **2007**, *46*, 5284−5304.
(37) Lane, T. J.; Nakagawa, I.; Walter, J. L.; Kandathil, A. J. Infrared investigation of certain imidazole derivatives and their metal chelates. *Inorg. Chem.* **1962**, *1*, 267−276.
(38) Morgan, K. J. The infrared spectra of some simple benzimidazoles. *J. Chem. Soc.* **1961**, 2343−2347.
(39) Malek, K.; Puc, A.; Schroeder, G.; Rybachenko, V. I.; Proniewicz, L. M. FT-IR and FT-Raman spectroscopies and DFT modelling of benzimidazolium salts. *Chem. Phys.* **2006**, *327*, 439−451.
(40) Edwards, S. J.; Soudackov, A. V.; Hammes-Schiffer, S. Analysis of kinetic isotope effects for proton-coupled electron transfer reactions. *J. Phys. Chem. A* **2009**, *113*, 2117−2126.
(41) Hammes-Schiffer, S. Proton-coupled electron transfer: Classification scheme and guide to theoretical methods. *Energy Environ. Sci.* **2012**, *5*, 7696−7703.
(42) Layfield, J. P.; Hammes-Schiffer, S. Hydrogen tunneling in enzymes and biomimetic models. *Chem. Rev.* **2014**, *114*, 3466−3494.
(43) Zhang, M.-T.; Irebo, T.; Johansson, O.; Hammarström, L. Proton-coupled electron transfer from tyrosine: A strong rate dependence on intramolecular proton transfer distance. *J. Am. Chem. Soc.* **2011**, *133*, 13224−13227.
(44) Hammes-Schiffer, S.; Soudackov, A. V. Proton-coupled electron transfer in solution, proteins, and electrochemistry. *J. Phys. Chem. B* **2008**, *112*, 14108−14123.
(45) Venkataraman, C.; Soudackov, A. V.; Hammes-Schiffer, S. Theoretical formulation of nonadiabatic electrochemical proton-coupled electron transfer at metal−solution interfaces. *J. Phys. Chem. C* **2008**, *112*, 12386−12397.
(46) Navrotskaya, I.; Soudackov, A. V.; Hammes-Schiffer, S. Model system-bath Hamiltonian and nonadiabatic rate constants for proton-coupled electron transfer at electrode-solution interfaces. *J. Chem. Phys.* **2008**, *128*, 244712.
(47) Ludlow, M. K.; Soudackov, A. V.; Hammes-Schiffer, S. Electrochemical proton-coupled electron transfer of an osmium aquo complex: Theoretical analysis of asymmetric Tafel plots and transfer coefficients. *J. Am. Chem. Soc.* **2010**, *132*, 1234−1235.
(48) Hammes-Schiffer, S.; Hatcher, E.; Ishikita, H.; Skone, J. H.; Soudackov, A. V. Theoretical studies of proton-coupled electron transfer: Models and concepts relevant to bioenergetics. *Coord. Chem. Rev.* **2008**, *252*, 384−394.
(49) Auer, B.; Fernandez, L. E.; Hammes-Schiffer, S. Theoretical analysis of proton relays in electrochemical proton-coupled electron transfer. *J. Am. Chem. Soc.* **2011**, *133*, 8282−8292.
(50) Horvath, S.; Fernandez, L. E.; Soudackov, A. V.; Hammes-Schiffer, S. Insights into proton-coupled electron transfer mechanisms of electrocatalytic H_2 oxidation and production. *Proc. Natl. Acad. Sci. U. S. A.* **2012**, *109*, 15663−15668.
(51) Hammes-Schiffer, S.; Stuchebrukhov, A. A. Theory of coupled electron and proton transfer reactions. *Chem. Rev.* **2010**, *110*, 6939−6960.
(52) Rhile, I. J.; Markle, T. F.; Nagao, H.; DiPasquale, A. G.; Lam, O. P.; Lockwood, M. A.; Rotter, K.; Mayer, J. M. Concerted proton−electron transfer in the oxidation of hydrogen-bonded phenols. *J. Am. Chem. Soc.* **2006**, *128*, 6075−6088.
(53) Glover, S. D.; Parada, G. A.; Markle, T. F.; Ott, S.; Hammarström, L. Isolating the effects of the proton tunneling distance on proton-coupled electron transfer in a series of homologous tyrosine-base model compounds. *J. Am. Chem. Soc.* **2017**, *139*, 2090−2101.
(54) Young, K. J.; Brennan, B. J.; Tagore, R.; Brudvig, G. W. Photosynthetic water oxidation: Insights from manganese model chemistry. *Acc. Chem. Res.* **2015**, *48*, 567−574.
(55) Machan, C. W.; Sampson, M. D.; Chabolla, S. A.; Dang, T.; Kubiak, C. P. Developing a mechanistic understanding of molecular electrocatalysts for CO_2 reduction using infrared spectroelectrochemistry. *Organometallics* **2014**, *33*, 4550−4559.
(56) Zavarine, I. S.; Kubiak, C. P. A versatile variable temperature thin layer reflectance spectroelectrochemical cell. *J. Electroanal. Chem.* **2001**, *495*, 106−109.
(57) Pavlishchuk, V. V.; Addison, A. W. Conversion constants for redox potentials measured versus different reference electrodes in acetonitrile solutions at 25 °C. *Inorg. Chim. Acta* **2000**, *298*, 97−102.

DOI: 10.1021/acscentsci.7b00125
ACS Cent. Sci. 2017, 3, 372−380